Flow-3D Numerical Modeling of Converged Side Weir

Article *in* Iranian Journal of Science and Technology - Transactions of Civil Engineering · May 2023

DOI: 10.1007/s40996-023-01077-y

CITATIONS
2

READS
125

4 authors:

Somayyeh Saffar

2 PUBLICATIONS **12** CITATIONS

SEE PROFILE

Abbas Safaei

Islamic Azad University, Shoushtar Branch

12 PUBLICATIONS **41** CITATIONS

SEE PROFILE

Farnoosh Aghaee Daneshvar

Shiraz University of Technology

14 PUBLICATIONS **48** CITATIONS

SEE PROFILE

Mohsen Solimani Babarsad

Islamic Azad University, Shoushtar Branch

27 PUBLICATIONS **82** CITATIONS

SEE PROFILE

Iranian Journal of Science and Technology, Transactions of Civil Engineering
https://doi.org/10.1007/s40996-023-01077-y

RESEARCH PAPER

Flow-3D Numerical Modeling of Converged Side Weir

Somayyeh Saffar[1] · Abbas Safaei[1] · Farnoush Aghaee Daneshvar[1] · Mohsen Solimani Babarsad[1]

Received: 9 January 2023 / Accepted: 19 February 2023

Abstract
A Side weir is used to divert water for various purposes in channels and rivers. In this study, the side weir is investigated in the converging section to increase the efficiency of this structure. This research has been done numerically and experimentally. Different geometric parameters have been considered for the side weir, including five weir lengths, four weir crest heights, two convergence angles, and three widths for the weir downstream channel. The range of flow changes in these experiments is from 10 to 100 cubic meters per hour. Flow-3D Software was used for numerical simulation. Comparing this software's results and laboratory data showed that Flow-3D could estimate water depth with R2 = 0.98. In this study, water surface and velocity profiles were investigated. After comparing converging and prismatic channels, it was found that reducing the downstream channel's width increased water depth and specific energy upstream. As a result, water can be diverted from the side weir even at low discharge.

Graphical Abstract

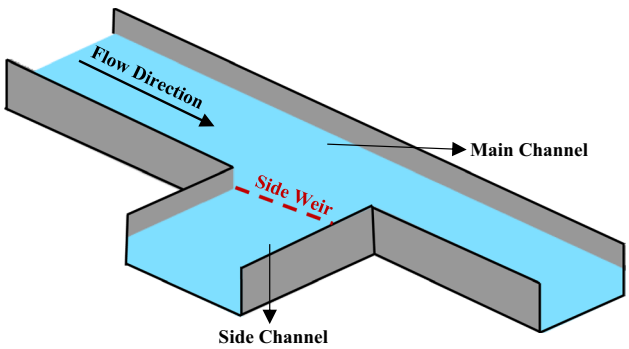

Keywords Side Weir · Converging · Flow-3D

1 Introduction

Weirs are essential structures widely used in hydraulic engineering and environmental application. As a typical weir, a side weir provides the ability to release excess or flood water in storage structures and control the discharge in the conveyance channels and irrigation systems. Spatially varied flow with decreasing discharge in the main channel is the dominant flow in side weirs. Numerous studies on hydraulic characteristics of the side weir flow field have been conducted to determine the discharge coefficient of this structure. The conditions of the side weir structure and how installed in the channel wall significantly affect the hydraulic characteristics of the flow. Researchers have always tried to increase the side weir's performance by changing the channel's geometry and shape of the side weir (Borghei & Parvaneh 2011; Abbasi et al. 2021; Kassaye 2022; Kartal & Emiroglu 2022; Granata et al. 2019).

Regarding three-dimensional and complex flow patterns passing through a side weir in the side channel, many studies have been accomplished on the shape, design, structure, free surface profile, and hydraulic properties of the side weirs.

✉ Mohsen Solimani Babarsad
mohsen.solb@iau.ac.ir

[1] Islamic Azad University Shoushtar, Shoushtar, Iran

Published online: 02 May 2023

The first experimental study on a side weir was performed by Engels (1920) and then, by Coleman and Smith (1923). Following the detailed studies of Forchheimer (1930), an analytical method was proposed assuming that the energy line was parallel to the crest of the weir and the channel bottom. For the first time, De Marchi (1934) proposed the simplified equation of spatially varied flow with decreasing discharge, again assuming that energy is constant along the weir and friction can be ignored for the rectangular horizontal channel. Ackers (1957) suggested the discharge coefficient value when the flow depth amount was measured along the axis close to the outer wall. Subramanya and Awasthy (1972) studied the discharge coefficient of the side weirs under supercritical and subcritical conditions. They showed that the flow energy loss due to the presence of a side weir at the beginning of the weir is negligible. Hager (1987) studied a side weir with the weir in the direction of flow with similar conditions and observed that the amount of specific energy in the side weir is more than ordinary weir, and the flow depth in this type of weir is almost equal to the amount of specific energy in ordinary weir. Bremen and Hager (1989) studied the flow in the side channel with a rectangular cross section in drainage channels. Their studies investigated the effect of non-prismatic cross section and bed slope on free water surface profiles. According to their results, the difference between the surface profiles of the channel axis and the side walls is partial in the subcritical flow. Also, different flow states, such as supercritical inflow conditions and the possibility of hydraulic jump formation along the flow, are discussed. In addition, Hager (1999) introduced the basic concepts and governing equations in the flow field of the side channels.

Due to the costly construction of physical models and laboratory equipment, computational and mathematical methods are widely used to model the flow of the side channel. *Computational fluid dynamics* (CFD) methods can calculate the water surface profile, velocity profile, and flow pattern along a side weir. Qu (2005) simulated the free surface flow on a side weir using the K-ε turbulence model and the volume of fluid (VOF) method. He compared his numerical model with the laboratory results of Subramanya and Awasthy (1972) and concluded that the *stagnation point* occurs near the downstream edge of the side weir. Mangarulkar (2010), using ANSYS ICEM, numerically simulated the free surface flow of a side weir with zero crest height using the K-ε and RNG turbulence models. Aydin (2012) simulated the flow field on a triangular labyrinth sharp-crested weir with different turbulence models. He concluded that the RSM turbulence model simulated fluctuations on the labyrinth side weir better than other turbulence models.

On the other hand, Al-Hashemi et al. (2017) performed laboratory and numerical studies on a broad-crested rectangular side weir with the FLUENT software to simulate the hydraulic phenomenon of its spatially varied flow and concluded that the K-ε turbulence model had an appropriate accuracy. Shaymaa et al. (2017a) studied a stepped broad-crested weir with a CFD turbulence model. He compared the flow discharge of each model and concluded that the K-ε model had the lowest error rate among the other models. Following the previous results, Shaymaa et al. (2017b) compared 2-D and 3-D simulations of the free surface flow on the broad-crested weir, using the K-ε turbulence model, which equal accuracy observed in both states. In addition to the studies mentioned on the broad-crested weir, scientists such as Kirkgov et al. (2008), Hoseini et al. (2013), Khassaf et al. (2016), and Shaker and Sarhan (2017) have also performed experiments on this field. Shaker and Jihan (2016) predicted water surface profiles by FLOW-3D and HEC-RAS software, concluding that FLOW-3D could be estimated more accurately than the other software. In addition, Afshar and Hoseini (2013) compared a rectangular broad-crested weir with a rounded corner by the FLOW-3D and three RNG K-ε, standard K-ε, and LES turbulence models to find the water level profile and streamlines together with laboratory model. Results indicated that the RNG K-ε model has the lowest errors. Also, Flow-3D has been used for evolving a relationship to estimate the discharge coefficient for rectangular sharp-crested weirs and examine velocity vectors and pressure patterns (Rady, 2011).

Investigation of the side weir flow properties and hydrodynamic parameters has essential effects on the free surface flow evaluations. The importance of the velocity distribution, discharge coefficient, and stagnation point position of the side weir flow was discussed frequently in the literature. Bagheri and Heidarpour (2011) measured the distribution of different velocity components and outflow discharge of a side weir experimentally. They concluded that the stagnation point occurred at the end of the side weir. Mangarulkar (2010) compared the location of the stagnation point obtained from the analytical study with the results of the numerical simulation. In addition, Mahmodinia et al. (2012) investigated the effect of inlet velocity on the free surface flow of the side weir while keeping the inlet depth constant. They concluded that the stagnation point moves upstream as the Froude number increases. Azimi et al. (2016) investigated the discharge coefficient of a rectangular side weir in a circular channel. A comparison between the laboratory and numerical models showed that the numerical model had acceptable accuracy. Savage et al. (2016) utilized physical and numerical models for labyrinth weirs with a 15° sidewall oblique angle to provide practical design in high headwater ratios. Maranzoni et al. (2017) performed an experimental and one-dimensional numerical study of the

flow on a side weir in the converging channel. They concluded that the side weir in a converging channel could be more efficient than a conventional channel.

Due to the complexity of the side weir and spatially varied flow, the idea of weir in the convergence section is considered. In this study, the side weir structure has been used in the converging section to evaluate the increase in the side weir efficiency (the ratio of water divert volume to general side weir). The effect of the weir angle on the weir function was investigated in the physical-hydraulic model, which was built in the hydraulic laboratory. An extensive research paper explored the measured experimental results (Saffar et al. 2021). In order to examine the performance of the weir structure, the FLOW-3D software is used to numerically simulate the side weir structure flow. Therefore, the velocity and flow depth distribution on the side weir in all directions are inspected accurately to investigate the effective length and proper width ratio for increasing the head of water on the side weir crest. Finally, the results of numerical simulation and physical modeling are compared to consider the appropriate hydraulic properties of the side weir.

2 Experimental Setup

The experiments were performed in the laboratory of Khuzestan Water and Power Authority (KWPA) in a flume 700 mm long, 310 mm wide, and 480 mm high. Discharge value and flow depth are measured using an electromagnetic flow meter and point gauge. Based on scenarios, 33 tests were done to study the weir in the laboratory.

Figure 1 shows a schematic of the side weir model. As shown in Fig. 1, B refers to the width of the upstream, b refers to the width of the downstream, L is the length of the side weir, and w is the weir crest height. Figure 2 shows the model setup.

3 Dimensional Analysis

The diverted flow (Q_w) is dependent on the hydraulic conditions and the geometric parameters of the side weir, so it can be written as follows:

$$Q_w = f_1\left(g.\sigma.\rho.H.h.L.w.B.b.Q_0\right) \tag{1}$$

where g is the gravity acceleration, ρ is the water density, μ is the water viscosity, σ is the water surface tension force,

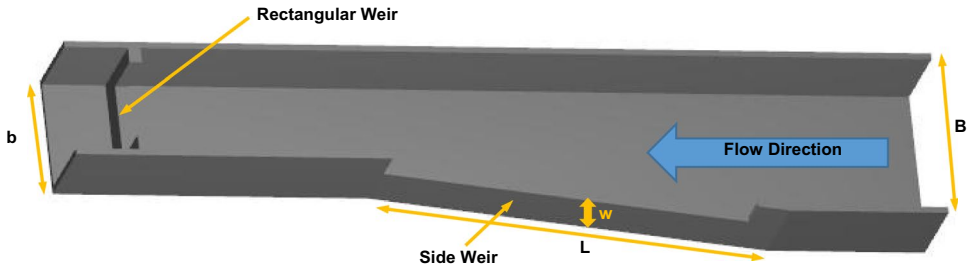

Fig. 1 Schematic plan of model

Fig. 2 View of the side weir physical model (upstream to downstream)

H is the water depth upstream the weir, h is water height on the weir, and Q_0 is the inflow.

Using Buckingham's Π-theorem and ignoring the effect of viscosity and surface tension, changed the above equation as follows:

$$\frac{Q_w}{Q_0} = \left(F_r.\frac{b}{B}.\frac{H}{B}.\frac{h}{b}.\frac{w}{H}.\frac{w}{L}.\frac{w}{b}.\frac{H}{w}.\frac{B-b}{L}.\frac{w}{B}\right) \tag{2}$$

$\frac{Q_w}{Q_0}$ Is referred to the ratio of the diverted flow.

4 Numerical Model

Flow-3D model is one of the most powerful software in the field of fluid mechanics that was developed and supported by Flow Science, Inc. This software has a high ability in water flow, sediment transfer, and hydrodynamic scouring simulation and is suitable for hydraulic simulations. The use of the Volume of Fluid Method (VOF) method for fluid surface prediction, its combination with the FAVOR method in detecting rigid boundaries, and the use of a simple rectangular cube solution network are the features of this model that distinguishes it from similar soft wares.

5 Governing Equations

FLOW-3D uses continuity equation (Eq. 3) and Reynolds-Averaged Navier–Stokes (RANS) equations (Eq. 4) to solve the flow equations:

$$\frac{\partial U_i}{\partial x_i} = 0 \tag{3}$$

$$\frac{\partial U_i}{\partial t} + U_j\frac{\partial U_i}{\partial x_j} = \frac{1}{\rho}\frac{\partial}{\partial x_j}\left[-P\delta_{ij} + \rho v_t\left(\frac{\partial U_i}{\partial x_j} + \frac{\partial U_j}{\partial x_i}\right)\right] \tag{4}$$

where U is the Reynolds-averaged velocity over time t, x is the spatial geometrical scale, ρ is the water density, P is the Reynolds-averaged pressure,δ Kronecker delta, and v_T is the turbulent eddy-viscosity.

Also, in this numerical study, VOF is used to predict the changes in the free flow surface to calculate the volumetric component of the fluid expressed by Hirth and Nicols (1981) (Eq. 5):

$$\frac{\partial F}{\partial t} + u\frac{\partial F}{\partial x} + v\frac{\partial F}{\partial y} = 0 \tag{5}$$

where u and v are fluid velocity components in the x and y coordinate direction. Here, F is the volumetric component of the fluid, if it is full of water in a given computational cell, then F = 1. If F = 0, the cell is empty, and if 0 < F < 1, the given cell contains both phases of air and water.

6 Turbulence Model

K-ε turbulence model (RNG) was first proposed by Yakhut et al. (2002). This model is defined by the following two equations:

$$\rho\frac{\mathrm{D}k}{\mathrm{D}t} = \frac{\partial}{\partial x_i}\left[a_k\mu_{\mathrm{eff}}\frac{\partial k}{\partial x_i}\right] + G_k + G_b - \rho\varepsilon \tag{6}$$

$$\rho\frac{\mathrm{D}\varepsilon}{\mathrm{D}t} = \frac{\partial}{\partial x_i}\left[a_s\mu_{\mathrm{eff}}\frac{\partial \varepsilon}{\partial x_j}\right] + C_{1\varepsilon}\frac{\varepsilon}{k}\left(G_k + G_{3\varepsilon}G_b\right) - C_{2\varepsilon}\rho\frac{\varepsilon^2}{k} \tag{7}$$

In these equations, k is the turbulent kinetic energy; ε is the turbulence dissipation rate,G_k is production of turbulent kinetic energy due to velocity gradient, G_b is turbulent kinetic energy, a_s and a_k invert the Prandtl-Number. a_k,a_s, $C_{1\varepsilon,}$ and $C_{2\varepsilon}$ are model constants. μ_{eff} is refer to effective viscosity that is the sum of turbulent viscosity and molecular viscosity. μ_{eff} is obtained from the following equations:

$$d\left(\frac{\rho^2 k}{\sqrt{\varepsilon\mu}}\right) = 1.72\frac{\nu}{\sqrt{\nu^3 - 1 + C_\nu}} \tag{8}$$

$$\nu = \frac{\mu_{\mathrm{eff}}}{\mu}.C_\nu = 100 \tag{9}$$

7 Numerical Setup

In this study, to model the side weir in FLOW-3D, a three-dimensional model file was drawn in AutoCAD. Then, it is saved as an STL file and called in FLOW-3D. The method of running software is such that the required data, such as shape, determination of simulation time, type of fluid, determination of the type of turbulence equations, simulate the model, and finally, the results are compared with physical data on the side weir. The turbulence model used in this study is K-ε (RNG) Fig. 3. The reason for using this turbulence model, in addition to the suggestions of previous research, is the excellent compatibility of the model with rotational flows and flows with large strains. In this study, the flow is continuous and turbulent, and incompressible fluid is considered.

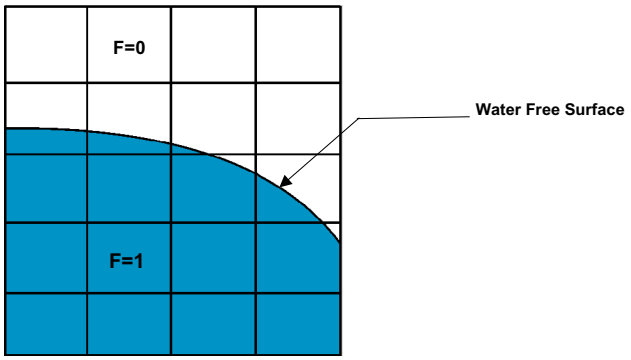

Fig. 3 Empty and fully cells water fraction (F)

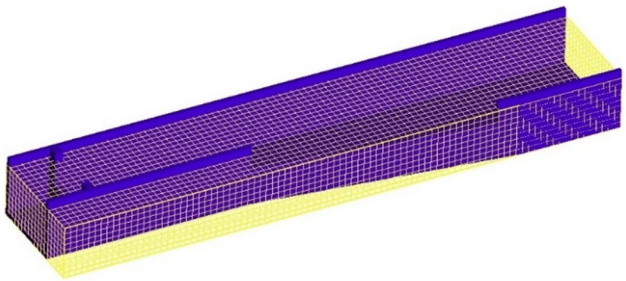

Fig. 4 Mesh view

7.1 Grid Types and Generation

One of the important topics that should be considered for simulation is determining computational networks. Since the density of the mesh dramatically affects the accuracy of the results and computational time, it is necessary to adopt a suitable mesh that meets both the accuracy required for calculations and is normal in terms of calculation time. The size of the meshes is selected in three coordinate directions of 1 cm. The number of cells varies depending on the model and its size. Figure 4 shows a schematic of the mesh on the side weir in software.

7.2 Boundary Conditions

Discharge boundary condition (volume flow rate) has been used at the inlet section ($X_{\min}$) to determine boundary conditions. A specific discharge is defined as the inflow that is injected uniformly over the flume's entire surface. On the side of the walls ($Y_{\min}$, $Y_{\max}$) and the channel bed ($Z_{\min}$), given that the velocity of the fluid on the solid boundaries is equal to zero, the wall boundary condition is used. In the case of a wall, the wall's surface is considered smooth, while in the laboratory, the wall was made of glass. The symmetry condition is used at the upper boundary of the weir ($Z_{\max}$). Also, the outflow condition has been used in the outflow section ($X_{\max}$).

The turbulence kinetic energy ($K_{0)}$ and the rate of kinetic energy dissipation (ε_0) are also calculated by the following equations:

$$K_0 = \frac{3}{2}\left(T_U U_0\right)^2 \tag{10}$$

$$\varepsilon_0 = C_\mu^{3/4}\frac{K^{3/2}}{l} \tag{11}$$

where T_U called the intensity of inflow turbulence with a value between 1 and 6%. C_μ is the experimental constant equal to 0.09, and l is the turbulence length.

7.3 Time Step

A stability criterion used in software Flow-3D to calculate the maximum interval size is Courant-type. Courant number determines how fast fluid can pass through a cell. If Courant number is greater than one, it means that the velocity of the particles is too high to pass over a period of time. In this study, time steps have been selected 0.01 s.

8 Result

8.1 Verification of Numerical Model and Laboratory Results

One of the methods to validate and compare the results as well as determine the range of error percentage between the data obtained from FLOW-3D with laboratory data is to use Eq. (12) to determine the relative error:

$$E = \frac{100}{N}\sum_{i=1}^{n}\left|\frac{(H)_{\mathrm{EXP}} - (H)_{\mathrm{NUM}}}{(H)_{\mathrm{EXP}}}\right| \tag{12}$$

In Eq. (12), E represents the percentage of absolute mean error; N is the number of laboratory data, $(H)_{\mathrm{EXP}}$ is the

Table 1 per cent error of water depth upstream between Experimental data and Flow-3D results

E(%)	$(H)_{\mathrm{EXP}}$(cm)	$(H)_{\mathrm{NUM}}$(cm)	$\frac{w}{L}$	$\frac{w}{b}$	$\frac{b}{B}$
0	22.7	22.7	0.167	1.28	0.483
4.4	15.7	16.4	0.122	0.933	0.483
2.6	18.9	18.4	0.143	0.785	0.677
1.9	`15.9	16.2	0.122	0.778	0.581
1	19.2	19.0	0.143	0.917	0.581
3	19.7	19.1	0.173	0.917	0.581
2.1	19	18.6	0.173	0.785	0.677

amount of flow depth measured, and $(H)_{NUM}$ is the amount of flow depth obtained from the numerical solution. In this study, the results related to the flow surface profile obtained from the software FLOW-3D have been compared and validated with laboratory results. Table 1 shows the results of several simulations for different dimensions and discharges. Also, the percentage of relative error of the results of numerical and experimental test data in each tested state is presented in Table 1.

The software provides the data with reasonable accuracy, and flow can be investigated on the side weir with less hydraulic cost and energy. On average, it can be said that the relative error for estimating the water depth of the upstream weir is 1.84%. Figure 5 shows the model implemented in Flow-3D.

8.2 Longitudinal Profile of Water Surface

To understand the effect of the side weir on the longitudinal profile of the water surface, under different geometric and hydraulic conditions, the profiles were drawn for the middle of the main channel by the software Flow-3D. (Fig. 6) In different geometric states of the model and under different hydraulic conditions, we do not observe a constant trend for the water surface profile, but the increasing and decreasing trend of the water surface profile is different in each state.

8.3 Transverse Profile of Water Surface

In Fig. 7, transverse profiles were drawn at the upstream, downstream, and middle of the side weir. Figure 8 shows the model plan where the sections are shown. Sections A, B, and C are at the upstream, middle, and downstream of the weir, respectively. The cross section A is 5 cm after the beginning of the weir, and the C cross section is 5 cm before the end. The convergence of the leading channel cause to shortening of graphs from start to end. According to Fig. 7, it can be seen that in side weirs, at the upstream and middle, the water surface profile has a descending slope, while at the end of the weir, it has an ascending slope. It can also be concluded that the maximum height of the water surface occurs at the end of the weir and in its vicinity.

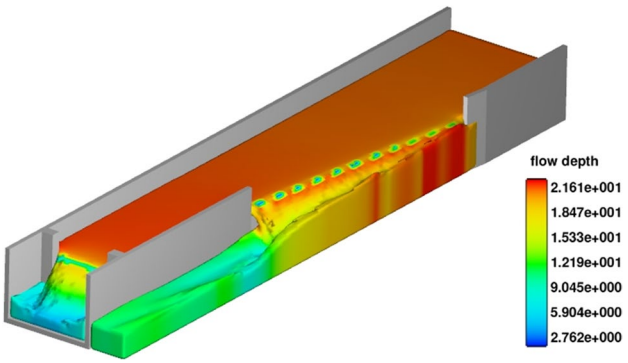

Fig. 6 Setup schematic and software boundaries

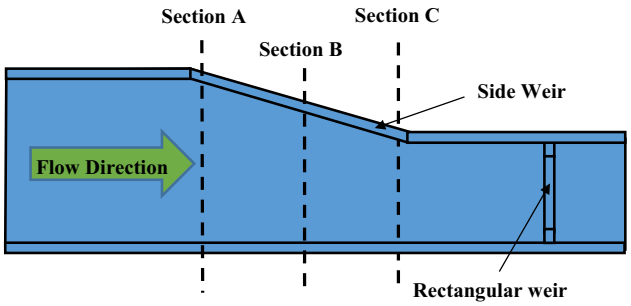

Fig. 7 Transverse profile of water surface

8.4 Effect of $\frac{b}{B}$ Ratio on Upstream Water Height

One of the advantages of channel convergence is that the changes in the water surface on the side weir are constantly related to the side weir in the straight section. By reducing

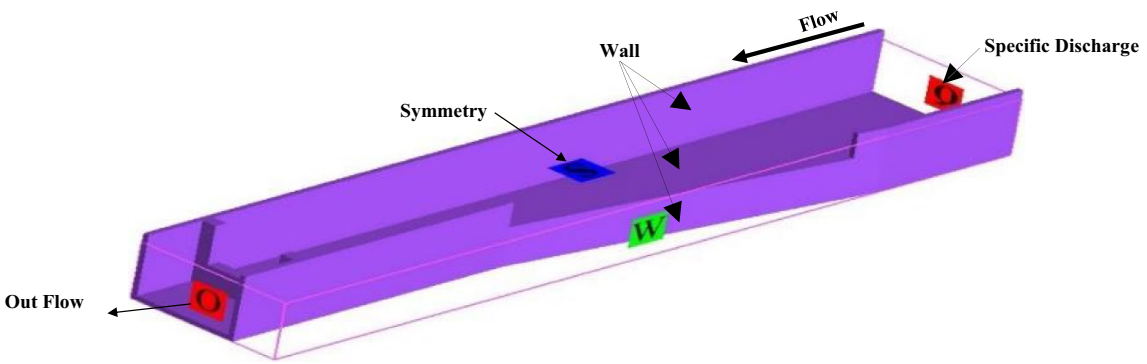

Fig. 5 Flow passing over side weir

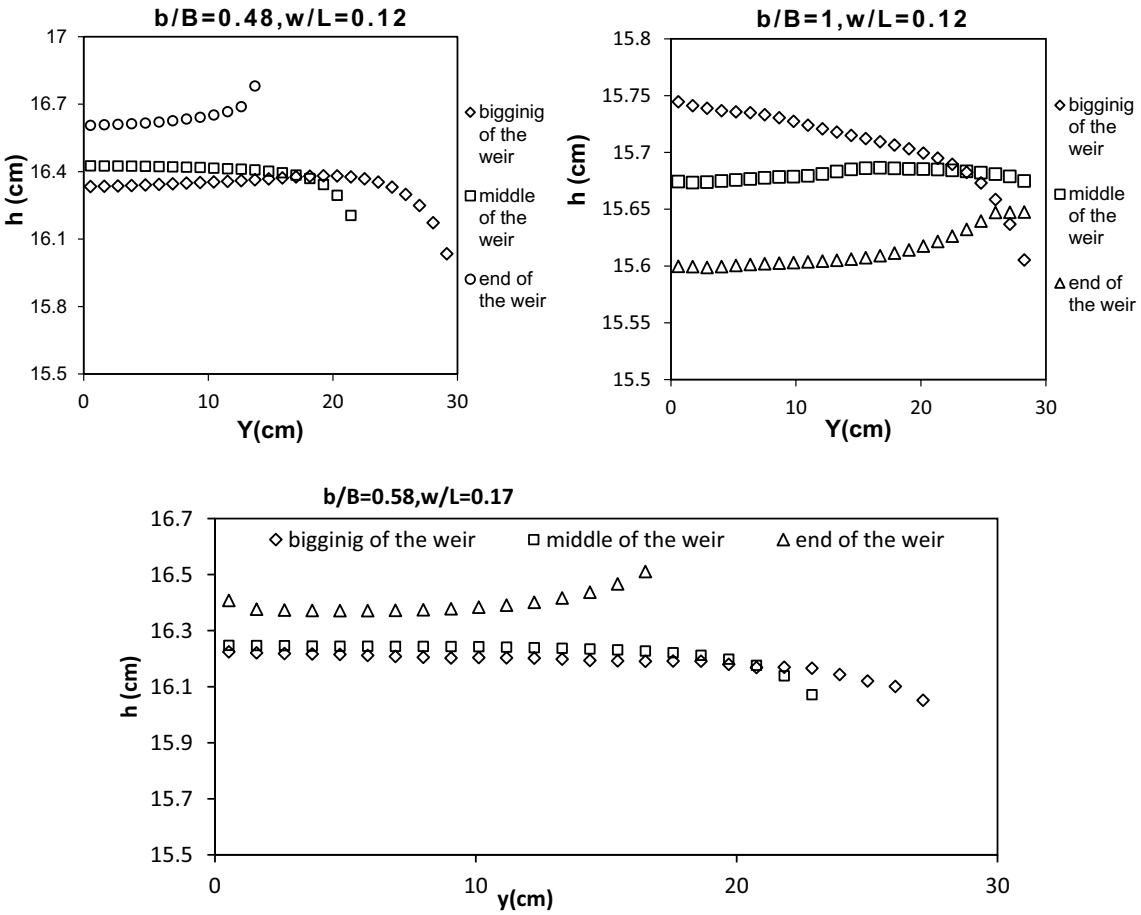

Fig. 8 Show sections in the plan

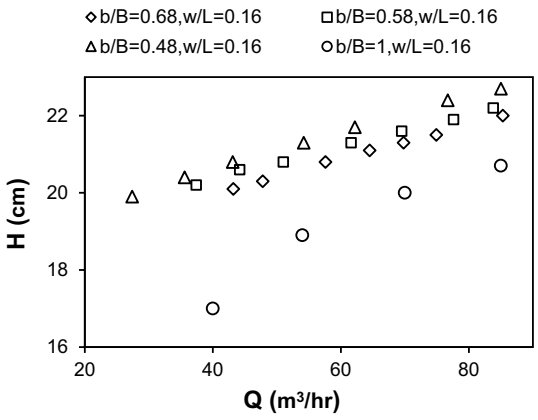

Fig. 9 Rating curves

the channel width downstream of the weir, the water surface in the channel and thus, on the side, weir rises. Figure 9 shows the rating curve of the side weir model with different b/B ratios. According to the curve, it can be seen that the smaller the b/B ratio, the water surface rises. For b/B = 0.48 compared to b/B = 1, the upstream water surface can be increased up to 12%.

8.5 The Effect of $\frac{b}{B}$ Ratio on Energy Loss

To analyze the effect of the $\frac{b}{B}$ ratio on the specific energy changes and the rate of energy loss along the channel, the ratio of upstream specific energy to downstream specific energy $\frac{E_d}{E_O}$ is plotted against the upstream Froude number Fr_o in Fig. 10. It is natural that the larger the $\frac{E_d}{E_O}$ ratio, the lower the energy loss, while if the $\frac{E_d}{E_O}$ ratio more significant than one, it means that there is energy retrieving during the flow. According to Fig. 10, for an identical Froude number, as the ratio of $\frac{b}{B}$ increases, the ratio of $\frac{E_d}{E_O}$ decreases, or in other words, the energy loss increases.

8.6 Velocity Profiles

According to the simulation results, the maximum longitudinal velocity in the converging channel occurs upstream of

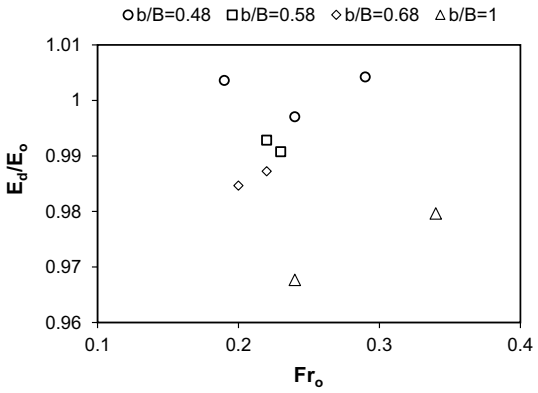

Fig. 10 Plot $\frac{E_d}{E_o}$ versus Fr_o for $\frac{b}{B}$ values

the side weir and in its vicinity. The maximum transverse velocity occurs on the side weir (Figs. 11 and 12). The maximum longitudinal and transverse velocity location is the same as the converging channel. (The positions of sections A, B, and C are shown in Fig. 8).

9 Conclusion

Numerical Investigation, most of the conducted studies are related to sharp and broad-crested weirs in the prismatic channel. At the same time, these side weirs have low efficiency despite their ease of implementation and design, and their calculation based on De Marchi equations is challenging. A practical way to solve this problem is to increase the side weir's effective length by converging the weir crest along the channel length. Another effective method to increase the efficiency of side weirs is increasing the head of water on the crest of the side weir and creating a backwater effect by decreasing downstream channel width. by converging the channel, the water rises on the weir, causing diversion discharge; as a result, the efficiency of water flowing out of the channel increases. By decreasing the ratio b/B, the energy loss along the side weir decreases, and the specific energy upstream of the side weir increases.

In addition, if the flow diversion from the side weir reduces downstream channel discharge, the constant width of the downstream channel can also be economically unjustifiable. Accordingly, a suitable alternative to improve side weir efficiency is to create a non-prismatic converging channel in the side weir range (apply a reduction state in the channel width and create an oblique weir) in the direction of the mainstream.

According to the study, the longitudinal profile of the water surface depends on hydraulic and geometric conditions of the channel and flow, and we have a unique profile for each model. However, the transverse profile of the water surface for different models is such that at the upstream and middle of the weir, the water surface profile has a descending trend, but at the end of the channel, it has an ascending trend. The location of the maximum longitudinal velocity occurs upstream of the side weir and in its vicinity, while

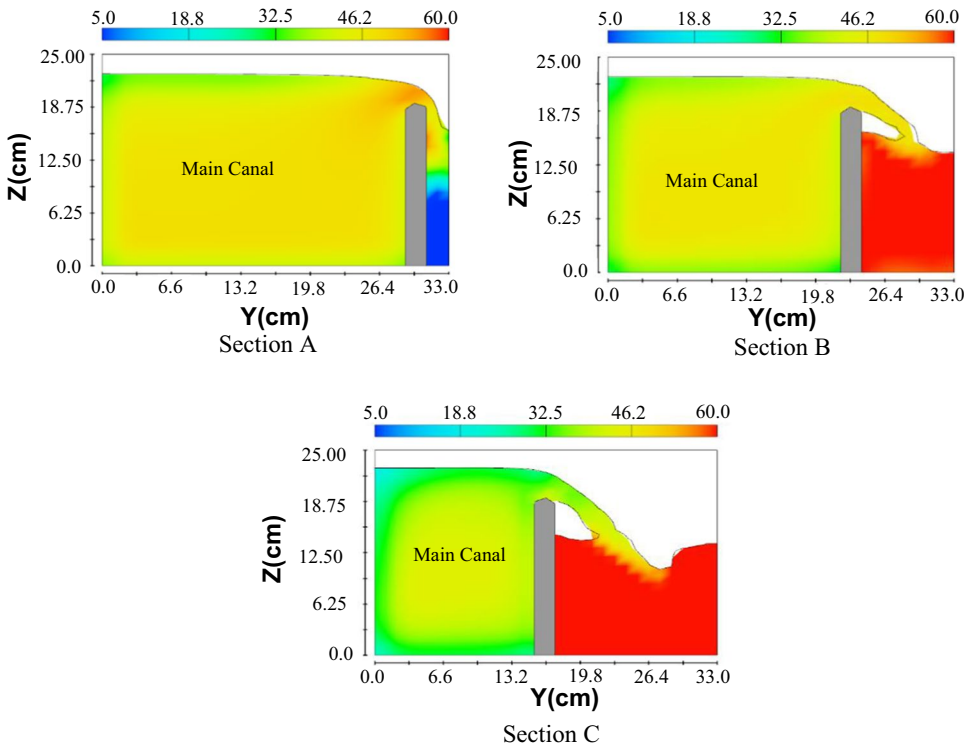

Fig. 11 2-D X-Velocity distribution through side weir for discharge 85 (m^3/hr), $\frac{b}{B} = 0.48$ and $\frac{w}{L} = 0.17$ in three sections

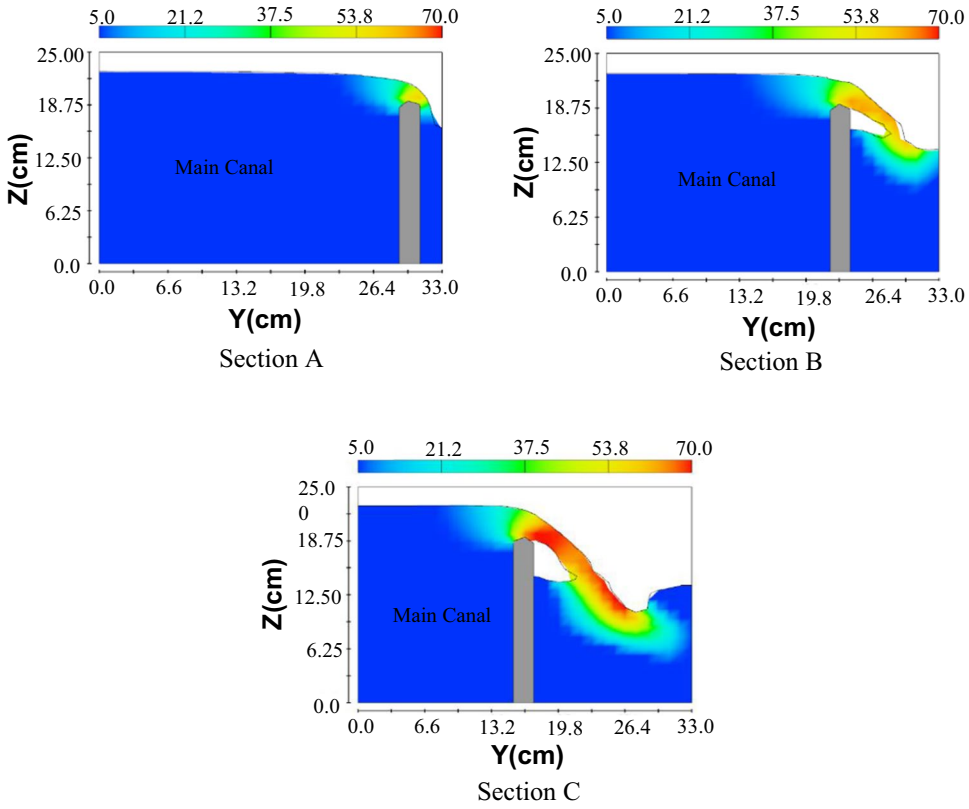

Fig. 12 2-D Y-Velocity distribution through side weir for discharge 85 (m^3/hr), $\frac{b}{B} = 0.48$ and $\frac{w}{L} = 0.17$ in three sections

the maximum transverse velocity for each section occurs on the side weir.

References

Abbasi S, Fatemi S, Ghaderi A, Di Francesco S (2021) The Effect of Geometric Parameters of the Antivortex on a Triangular Labyrinth Side Weir. Water 13(1):14. https://doi.org/10.3390/w13010014

Ackers P (1957) A Theoretical Consideration of Side-weirs as Storm Water Overflows. Proceeding of Institute of Civil Engineers 6:250–269

Afshar H, Hoseini SH (2013) Experimental and 3-D numerical simulation of flow over a rectangular broad- crested weir. International Journal of Engineering and Advanced Technology (IJEAT) 2(6):214–219

Al-Hashimi AS, Madhloom MH, Nahi NT (2017) Experimental and Numerical Simulation of Flow Over Broad Crested Weir and Stepped Weir using Different Turbulence Models. Journal of Engineering and Sustainable Development 21(2):28–45

Aydin MC (2012) CFD simulation of free-surface flow over triangular labyrinth side weir. Adv Eng Softw 45(1):159–166. https://doi.org/10.1016/j.advengsoft.2011.09.006

Azimi H, Shabanlou S, Ebtehaj I, Bonakdari H (2016) Discharge coefficient of rectangular side weirs on circular channels. International Journal of Nonlinear Sciences and Numerical Simulation 17(7–8):391–399. https://doi.org/10.1515/ijnsns-2016-0033

Bagheri S, Heidarpour M (2011) Characteristics of flow over rectangular sharp crested side weirs. J Irrig Drain Eng 138(6):541–547. https://doi.org/10.1061/(ASCE)IR.1943-4774.0000433

Borghei SM, Parvaneh A (2011) Discharge characteristics of a modified oblique side weir in subcritical flow. Flow Meas Instrum 22(5):370–376. https://doi.org/10.1016/j.flowmeasinst.2011.04.009

Bremen R, Hager WH (1989) Experiments in side channel spillways (Experimente Sammel kanalen). J Hydraul Eng ASCE 115(5):617–635

Coleman GS, Smith D (1923) The discharging capacity of side weirs. Proceeding of Institute of Civil Engineers 6(2):288–304

DeMarchi G (1934) Essay on the performance of lateral weirs. L'energia Electrica Milan 11(11):849–860

DurgaRao KHV, Pillai CRS (2008) Study of Flow Over Side Weirs in Supercritical Conditions. Water Resource Management 22:131–143. https://doi.org/10.1007/s11269-007-9153-4

Engels H (1920) Releases from the dresdner river engineering laboratory. Z Ver Dtsch Ing (in German) 64(5):101–106

Forchheimer P (1930) Hydraulics Teubner Verlagsgevellschaft, 3rd edn. Leibzig, Berlin

Granata F, Di Nunno F, Gargano R, de Marinis G (2019) Equivalent Discharge Coefficient of Side Weirs in Circular Channel—A Lazy Machine Learning Approach. Water 11(11):2406. https://doi.org/10.3390/w11112406

Hager WH (1987) Lateral outflow over side weirs. J Hydraulic Engineering 113(4):491–504. https://doi.org/10.1061/(ASCE)0733429(1987)113:4(491)

Hager WH (1999) Wastewater hydraulics theory and practice. Springer, Berlin Heidelberg New York

Hirt CW, Nichols BD (1981) Volume of fluid (VOF) method for the dynamics of free boundaries. J Comput Phys 39(1):201–225. https://doi.org/10.1016/0021-9991(81)90145-5

Hoseini SH (2013) Determination of Discharge Coefficient of Rectangular Broad Crested Side Weir in Trapezoidal Channel by CFD. International Journal of Hydraulic Engineering 2(4):64–70. https://doi.org/10.5923/j.ijhe.20130204.02

Kartal V, Emiroglu ME. (2022). Experimental analysis of combined side weir-gate located on a straight channel. Flow Measurement and Instrumentation. 88, 102250. https://doi.org/10.1016/j.flowmeasinst.2022.102250.

Kassaye AA, Mohammed AK, Angello ZA. (2022). Evaluation of the flow measurement performance of compound sharp-crested overfall weirs and optimized discharge measurement in data scarce areas. Water Resources, 49(3), 402–412. https://link.springer.com/article/https://doi.org/10.1134/S0097807822030034.

Khassaf SI, Attiyah AN, Yousify HA (2016) Experimental investigation of compound side weir with modelling using computational fluid dynamic. International Journal of Energy and Environment 7(2):169–178

Kirkgov MS, Akoz MS, Oner AP (2008) Experimental investigation of compound side weir with modelling using computational fluid dynamic. Canadian Journal of Civil Engineering. 35(9):975–986. https://cdnsciencepub.com/doi/https://doi.org/10.1139/L08-036.

Mahmodinia S, Javan M, Eghbalzadeh A (2012) The effects of the upstream Froude number on the free surface flow over the side weirs. Procedia Engineering 28:644–647. https://doi.org/10.1016/j.proeng.2012.01.784

Mangarulkar K (2010). Experimental and numerical study of the characteristics of side weir flows. Master Thesis, Concordia University, Montreal, Quebec, Canada.

Maranzoni A, Pilotti M, Tomirotti M (2017). Experimental and Numerical Analysis of Side Weir Flows in a Converging Channel. Journal of Hydraulic Engineering, 143(7). https://ascelibrary.org/doi/https://doi.org/10.1061/%28ASCE%29HY.1943-7900.0001296.

Qu J (2005). Three-dimensional turbulence modeling for free surface flows. PhD thesis, Concordia University.

Rady A-H, RM. (2011) 2D–3D modeling of flow over sharp-crested weirs. J Appl Sci Res 7(12):2495–2505

Saffar S, Babarsad MS, Shooshtari MM, Poormohammadi MH, Riazi R (2021) Prediction of the discharge of side weir in the converge channels using artificial neural networks. Flow Meas Instrum 78:101889. https://doi.org/10.1016/j.flowmeasinst.2021.101889

Savage BM, Crookston BM, Paxson GS (2016). Physical and numerical modeling of large headwater ratios for a 15° labyrinth spillway. International Journal of Hydraulic Engineering 142(11). https://doi.org/10.1061/(ASCE)HY.1943-7900.0001186.

Shaker J, Jihan Q (2016) Numerical Modelling of Flow over Single-Step Broad- Crested Weir Using FLOW-3D and HEC-RAS. Polytechnic General Sciences Journal 6(3):435–448

Shaker J, Sarhan A (2017) Characteristics of hydraulic jump on a striped channel bed. J Duhok Univ 654–661

Shaymaa AM, Huda MM, Thameen NN (2017a) Experimental and numerical simulation of flow over broadcrested weir and stepped weir using different turbulence models. Eng Sustainable Dev 21(2):28–45

Shaymaa AM, Huda MM, Rasul MK, Thameen NN, Nadhir AA (2017b) Flow over broad-crested weirs: comparison of 2d and 3d models. Journal of Civil Engineering and Architecture 11(8):769–779. https://doi.org/10.17265/1934-7359/2017.08.005

Subramanya K, Awasthy SC (1972) Spatially varied flow over side weirs. J Hydraul Div 98(1):1–10

Yakhut V, Shock RA, Mallick S, Chen H, Zhang R (2002) Recent results on two-dimensional airfoils using a lattice Boltzmann-based algorithm. J Aircr 39(3):434–439